14th International Symposium on Ballistics, Québec, Canada, 26-29 September 1993

PENETRATION OF EXPLOSIVES BY SHAPED-CHARGE JETS

Dr. William J. Flis* and Mr. Michael G. Crilly, Dyna East Corporation;
Mr. George Hodges, U.S. Army Test and Evaluation Command;
and Mr. Chuck Vessels, U.S. Army Missile Command

Shaped-charge penetration of explosives is studied analytically and experimentally. Two models are developed, each applicable to a different regime of jet velocity. The first addresses high-velocity penetration. If a jet is sufficiently fast, its penetration velocity will exceed the explosive's detonation velocity, and the process may achieve a steady state with the crater following the detonation wave. The model predicts that penetration per unit jet length is about 15% less than that predicted by the density law, a reduction similar to that predicted by the compressible theory for inert compressible materials.

A second model addresses slower penetrations where the detonation wave precedes the penetration process to consume all the explosive. Later, the explosive product gases may, if confined, reach equilibrium at a high pressure, and penetration may then achieve a steady state. This model, which applies compressible penetration theory to a target of ideal gas, predicts that, at low jet velocities, the initial high pressure of the gas greatly reduces the penetration. Comparison of this model with some experimental results shows excellent agreement provided foreshortening is taken into account.

INTRODUCTION

Shaped-charge jet penetration of an explosive charge is usually an unsteady process. When the jet first penetrates, the explosive starts to react, and soon the reaction propagates into the explosive, possibly as a detonation wave. Usually, the detonation wave has a velocity greater than the rate of penetration, and outruns the penetration process. In such a penetration, then, a steady state is generally not achieved.

However, if a jet is fast and dense enough (Case I), its penetration can keep up with the detonation wave, which stands as a bow wave ahead of the crater, and a steady state may be achieved. Such a penetration may be modeled following an approach developed for inert compressible materials[1,2]. This paper develops a model, outlines a solution method, and compares some sample calculations with experimental results.

Another situation (Case II) that may reach a steady state is when a confined explosive is initiated before the jet arrives, as when the initial impact drives a shock through the confinement with sufficient strength to set off the explosive. The confinement maintains the explosive pressure until penetration by the jet. A steady state may also develop when a jet has been penetrating a large body of explosive for some time. In either case, the result is that the jet encounters the explosive products in a quiescent state of high initial pressure. Except for very slow jets, there will be a standing shock wave in the gases ahead of the crater.

[1] B.S. Haugstad and O.S. Dullum, "Finite Compressibility in Shaped Charge Jet and Long Rod Penetration — The Effect of Shocks," *J. Appl. Phys.*, V. 52, no. 8, 1981.

[2] W.J. Flis and P.C. Chou, "Penetration of Compressible Materials by Shaped-Charge Jets," *Proc. 7th Inter. Symp. Ballistics,* The Hague, The Netherlands, 19-21 April 1983.

MODEL

This section describes a model of steady-state jet penetration into an explosive, with equations applicable to both Cases I and II. Figure 1(a) shows penetration by a jet, with velocity V, into a target at a rate U. For a steady state, the shock or detonation wave (which is generally overdriven) must stand in the target as a bow wave ahead of the crater. Thus, in a reacting explosive target, penetration must be rapid enough to keep up with the detonation. Also, if the jet velocity is great enough, a standing shock may exist where jet material enters its zone of active involvement in the penetration.

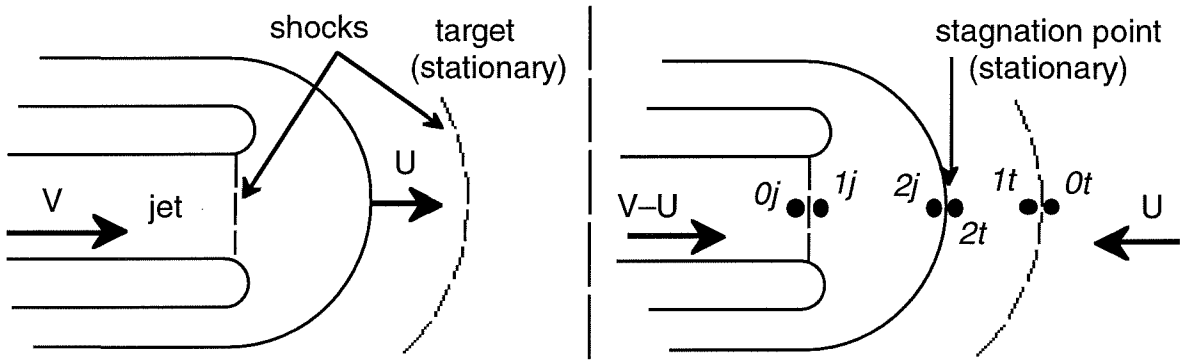

a) in stationary coordinates b) in moving coordinates

Figure 1. Steady-state jet penetration into explosive or explosive products.

Figure 1(b) shows the flow field in moving coordinates attached to the crater bottom, which appears as a stagnation point to both the jet and target. Jet material approaches this point at velocity (V – U), is suddenly decelerated and compressed by its standing shock (if one exists), and is then further decelerated and compressed on its way to the stagnation point. Target material approaches at velocity U, is likewise compressed and decelerated (and perhaps reacts, as well) on passing through its standing shock or detonation wave, and is then further compressed and slowed to the stagnation point.

To analyze this flow, we define, along the axial streamline in the target, a station *0t* in the undisturbed explosive ahead of the wave, station *1t* just behind the wave, and station *2t* at the stagnation point. Corresponding stations are defined in the jet: *0j* in the undisturbed material, *1j* just behind its shock (if any), and *2j* at the stagnation point. We now develop the equations relating the velocities and states at these stations.

Initial Conditions Let W represent the flow velocity (in the moving coordinates) at which material approaches the stagnation point; then, in the undisturbed regions,

$$W_{0t} = U \qquad W_{0j} = V - U \tag{1}$$

Cases I and II differ as to initial pressure in the target. In Case I, the reacting explosive has no pressure,

I: $$p_{0t} = 0 \tag{2}$$

while in Case II, the confined, already-reacted explosive has an initial pressure, which we estimate by requiring adiabatic equilibrium with the C-J point,

II: $$p_{0t} = p_{CJ}\,(v_{CJ}/v_0)^{\gamma} = p_{CJ}\,[\gamma/(\gamma+1)]^{\gamma} \tag{3}$$

The pressure in the undisturbed part of the jet is zero,

$$p_{0j} = 0 \tag{4}$$

Shock Equations Across shocks in the jet and target, changes in properties are described by the Rankine-Hugoniot relations:

Mass: $$\rho_0 W_0 = \rho_1 W_1 \tag{5}$$

Momentum: $$p_0 + \rho_0 W_0^2 = p_1 + \rho_1 W_1^2 \tag{6}$$

Energy: $$e_0 + \frac{1}{2} W_0^2 + \frac{p_0}{\rho_0} = e_1 + \frac{1}{2} W_1^2 + \frac{p_1}{\rho_1} \tag{7}$$

where e is specific internal energy. Equations (5) and (6) may be re-arranged as

$$W_1 = \rho_0 W_0 / \rho_1 \tag{8}$$

$$p_1 = p_0 + \rho_0 W_0^2 (1 - \rho_0/\rho_1) \tag{9}$$

which give W_1 and p_1 in terms of known quantities at station *0* and the ratio ρ_0/ρ_1.

Compressible Bernoulli's Equation As each material flows along the streamline from shock to stagnation point, it is continuously and adiabatically decelerated. Therefore, this flow is governed by the compressible Bernoulli's equation,

$$\frac{1}{2} W_1^2 + \frac{p_1}{\rho_1} = \frac{1}{2} W_2^2 + \frac{p_2}{\rho_2} - \int_1^2 p \, dv \tag{10}$$

Stagnation-Point Conditions In the moving coordinates, stations *2t* and *2j* are stagnation points: $$W_{2t} = W_{2j} = 0 \tag{11}$$

The final condition is pressure equilibrium across the interface

$$p_{2t} = p_{2j} \tag{12}$$

Equations of State A complete description of the behavior of each material requires either its equation of state, $p = p(\rho, e)$, or, across shocks, a definition of its Hugoniot.

Reactive Materials For explosives, we use the ideal-gas, or γ-law, equation of state,

$$e = pv/(\gamma - 1) - fq \tag{13}$$

where γ is the ratio of specific heats (assumed constant) of the explosive products, q is the heat of detonation, and f is the burn fraction, which is zero ahead of the detonation wave and equal to one behind (I: $f_0 = 0$, $f_1 = f_2 = 1$). In Case II of already-reacted explosive, f is everywhere equal to unity (II: $f_0 = f_1 = f_2 = 1$). Along the isentrope, pressure is related to specific volume v according to $p\, v^\gamma = \text{constant} = p_1 v_1^\gamma$.

Inert Materials Changes in state across shocks may be described by the Hugoniot, which we express in the usual relation of shock velocity U_s to particle velocity U_p,

$$U_s = c_0 + b\, U_p \tag{14}$$

where c_0 is the bulk sound speed and b is a constant. The flow velocities are related to these velocities by $W_0 = U_s$ and $W_1 = U_s - U_p$, so that

$$W_0 = c_0 + b(W_0 - W_1) \tag{15}$$

Along the isentrope, we use the Mie-Grüneisen equation of state,

$$p = p(\rho, e) = (1 - \Gamma\mu/2)\, p_h + \Gamma\rho e \tag{16}$$

where $\mu \equiv \rho/\rho_0 - 1$ and Γ is the Grüneisen parameter, assumed to depend on density according to $\Gamma\rho = \Gamma_0\rho_0 = \text{constant}$. In Eq. (16), $p_h = p_h(\rho)$ is the pressure on the

Hugoniot at the same density,

$$p_h = \rho_0 c_0^2 \eta/(1 - b\eta)^2 \tag{17}$$

where $\eta \equiv (v_0 - v)/v_0$.

Solution The above system of equations may be solved by the same scheme developed by Haugstad and Dullum for penetration of compressible materials. Combining the shock energy equation (7) with the Bernoulli equation (10) yields

$$\frac{p_0}{\rho_0} + \frac{1}{2} W_0^2 + e_0 = \frac{p_2}{\rho_2} + \frac{1}{2} W_2^2 + e_2$$

Applying this equation to each material yields

$$\frac{p_{0t}}{\rho_{0t}} + \frac{1}{2} U^2 + e_{0t} = \frac{p_{2t}}{\rho_{2t}} + e_{2t}; \quad \frac{1}{2}(V - U)^2 = \frac{p_{2j}}{\rho_{2j}} + e_{2j}$$

since $e_{0j} = 0$ and $p_{0j} = 0$ for an inert jet. Equating p_{2t} and p_{2j} yields

$$\left(\frac{V - U}{U}\right)^2 = \frac{\rho_{2t}}{\rho_{2j}} \left\{ 1 + \frac{p_{0t}/\rho_{0t} + e_{0t} - e_{2t}}{\frac{1}{2} U^2} \right\} + \frac{e_{2j}}{\frac{1}{2} U^2} \tag{18}$$

which is solved by successive substitution: given V, a value of U is guessed, and the right-hand side is evaluated using equations given below depending on the material types. Then an improved value of U is found from Eq. (18), and the process is repeated until convergence, which takes only a few iterations. Procedures are now described for evaluating Eq. (18) for each type of material in each Case.

Reacting Explosive (Case I) Conditions behind the detonation wave are found by solving Eqs. (7-9) and (13) with initial conditions (1), (2), and (4), which yields

$$\text{I:} \qquad \frac{\rho_{0t}}{\rho_{1t}} = \frac{v_{1t}}{v_{0t}} = \frac{1}{\gamma + 1}\left(\gamma - \sqrt{1 - \frac{D^2}{U^2}}\right) \tag{19}$$

where D is the detonation velocity, equal to $\sqrt{[2q(\gamma^2 - 1)]}$. By Eq. (9),

$$\text{I:} \qquad p_{1t} = \rho_{0t} U^2 \left(1 - \frac{v_{1t}}{v_{0t}}\right) = p_{CJ} \frac{U^2}{D^2}\left(1 + \sqrt{1 - \frac{D^2}{U^2}}\right)$$

where p_{CJ} is the Chapman-Jouguet pressure, equal to $\rho_0 D^2/(\gamma + 1)$, or $2\rho_0 q(\gamma - 1)$. The integral along the isentrope in the Bernoulli equation may be evaluated,

$$\int_{1t}^{2t} p\, dv = \int_{1t}^{2t} p_{1t}\left(\frac{v_{1t}}{v}\right)^{\gamma} dv = -\frac{p_{1t} v_{1t}}{\gamma - 1}\left[\left(\frac{p_{2t}}{p_{1t}}\right)^{(\gamma-1)/\gamma} - 1\right] \tag{20}$$

Then, Eq. (10) may be solved, using values at *1t* given by Eqs. (8), (9), and (19), for the stagnation pressure,

$$p_{2t} = p_{1t}\left[1 + \frac{\gamma - 1}{\gamma}\frac{W_{1t}^2}{2 p_{1t} v_{1t}}\right]^{\gamma/(\gamma-1)}$$

$$\text{I:} \qquad = p_{CJ}\left(\frac{U}{D}\right)^2\left[1 + \sqrt{1 - \left(\frac{D}{U}\right)^2}\right]\left[\frac{\gamma + 1}{2\gamma}\left(1 + \frac{\gamma - 1}{1 + \sqrt{1 - (D/U)^2}}\right)\right]^{\frac{\gamma}{\gamma-1}}$$

If $\gamma = 3$ (a good approximation for most high explosives), this is equal to

I: $$p_{2t} = p_{CJ}\left(\frac{U}{D}\right)^2\left[1+\sqrt{1-\left(\frac{D}{U}\right)^2}\right]\left[\frac{2}{3}\left(1+\frac{2}{1+\sqrt{1-(D/U)^2}}\right)\right]^{\frac{3}{2}}$$

This pressure may be compared with that predicted by the incompressible theory, $p_{2,incompressible} = \rho_{0t} U^2/2$, which, for $\gamma = 3$, equals $2p_{CJ} U^2/D^2$; thus, the stagnation pressure predicted by the present model is greater than that predicted by the incompressible theory by a factor of at least $\sqrt{2}$.

Reacted Explosive Products (Case II) Conditions behind the shock in an already-reacted explosive are found by solving Eqs. (7-9) and (13) with conditions (1) and (3), to yield

II: $$\frac{\rho_{0t}}{\rho_{1t}} = \frac{v_{1t}}{v_{0t}} = \frac{1}{\gamma+1}\left(\frac{2c_0^2}{U^2}+\gamma-1\right) \qquad (21)$$

where $c_0 = \sqrt{(\gamma p_0 v_0)}$ is the sound speed ahead of the shock. Then, again using Eq. (20), Eq. (10) may be solved for the stagnation pressure,

II: $$p_{2t} = p_{1t}\left[1+\frac{\gamma-1}{\gamma}\frac{W_{1t}^2}{2\,p_{1t}\,v_{1t}}\right]^{\gamma/(\gamma-1)}$$

where W_{1t} and p_{1t} are given by Eqs. (8) and (9) with Eq. (21).

Inert Materials Conditions at station *1* are found by solving Eqs. (8), (9), and (15),

$$W_1 = [W_0(b-1) + c_0]/b$$

$$\rho_1 = \rho_0 W_0 b\,/[W_0(b-1) + c_0]$$

$$p_1 = \rho_0 W_0 (W_0 - W_1)$$

The integral in Bernoulli's equation (10) is taken along the isentrope, $de = -p\,dv$. For the Mie-Grüneisen EOS, the isentrope cannot easily be expressed in explicit form and must be constructed numerically. To do this, we use the identity,

$$\left(\frac{\partial p}{\partial v}\right)_s = -\left[\left(\frac{\partial e}{\partial v}\right)_p + p\right]\Big/\left(\frac{\partial e}{\partial p}\right)_v$$

For the Mie-Grüneisen EOS, $(\partial e/\partial v)_p = e_h' - p_h'/\rho\Gamma$, and $(\partial e/\partial p)_v = 1/\rho\Gamma$, where $e_h(v)$ is the energy on the Hugoniot at the same volume and where $\rho\Gamma$ forms a constant. Therefore, the isentrope curve in the (p, v)-plane becomes

$$\left(\frac{dp}{dv}\right)_C = -\rho\Gamma\left(\frac{de_h}{dv} - \frac{1}{\rho\Gamma}\frac{dp_h}{dv} + p\right) = -\rho\Gamma\left\{\frac{d}{dv}\left[\left(\frac{\eta}{2\rho_0}-\frac{1}{\rho\Gamma}\right)p_h\right] + p\right\}$$

Since p_h is complicated, this is difficult to integrate exactly. However, since it has the form $dp/dv = -\rho\Gamma\,[g'(v) + p]$, with $g \equiv \left(\frac{\eta}{2\rho_0}-\frac{1}{\rho\Gamma}\right)p_h$, we integrate it numerically as

$$\int_v^{v+\Delta v}\frac{dp}{dv}\,dv = \int_v^{v+\Delta v} -\rho\Gamma g'(v)\,dv - \int_v^{v+\Delta v}\rho\Gamma p\,dv$$

$$p(v+\Delta v) - p(v) = -\rho\Gamma\,[g(v)]_v^{v+\Delta v} - \rho\Gamma\left(\frac{p(v+\Delta v)+p(v)}{2}\right)\Delta v$$

which may be re-arranged to the explicit formula

$$p(v+\Delta v) = \frac{p(v) - \rho\,\Gamma\,[g(v+\Delta v) - g(v) + p(v)\,\Delta v/2]}{1 + \rho\,\Gamma\,\Delta v/2}$$

This formula is applied step-wise from starting point (p_1, v_1) to the stagnation point, where the flow velocity W_2 vanishes, so that the equation

$$W_1^2/2 + p_1 v_1 + e_1 = p_2 v_2 + e_2$$

must be satisfied. Here, the specific volume is v_2; the internal energy e_2 may be determined from p_2 and v_2 by the equation of state, Eq. (13) or (16).

EXAMPLE CALCULATIONS

A few calculations using these two models are shown in Figs. 2 and 3, which are plots of the ratio of penetration per unit length of jet calculated by our models to that predicted by the incompressible density law, $P/L = \sqrt{(\rho_j/\rho_t)}$, which is derived, of course, from the incompressible Bernoulli equation. The deviation of each curve from unity represents the effects of the extra mechanisms taken into account in our models: compressibility and either detonation (Case I) or high initial pressure (Case II). Material properties are listed in Table 1.

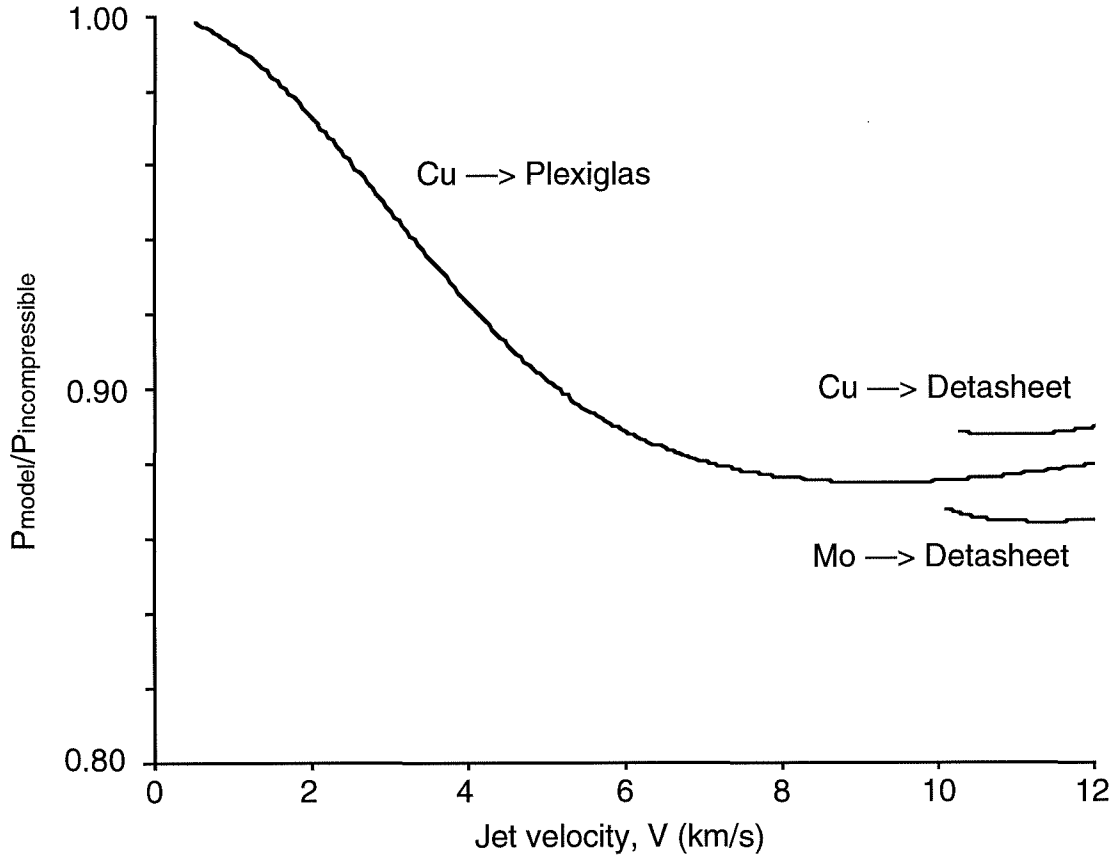

Figure 2. Model predictions of penetration per unit length of high-velocity jet into reacting explosive (Case I) and of Plexiglas, relative to the prediction of the incompressible density law.

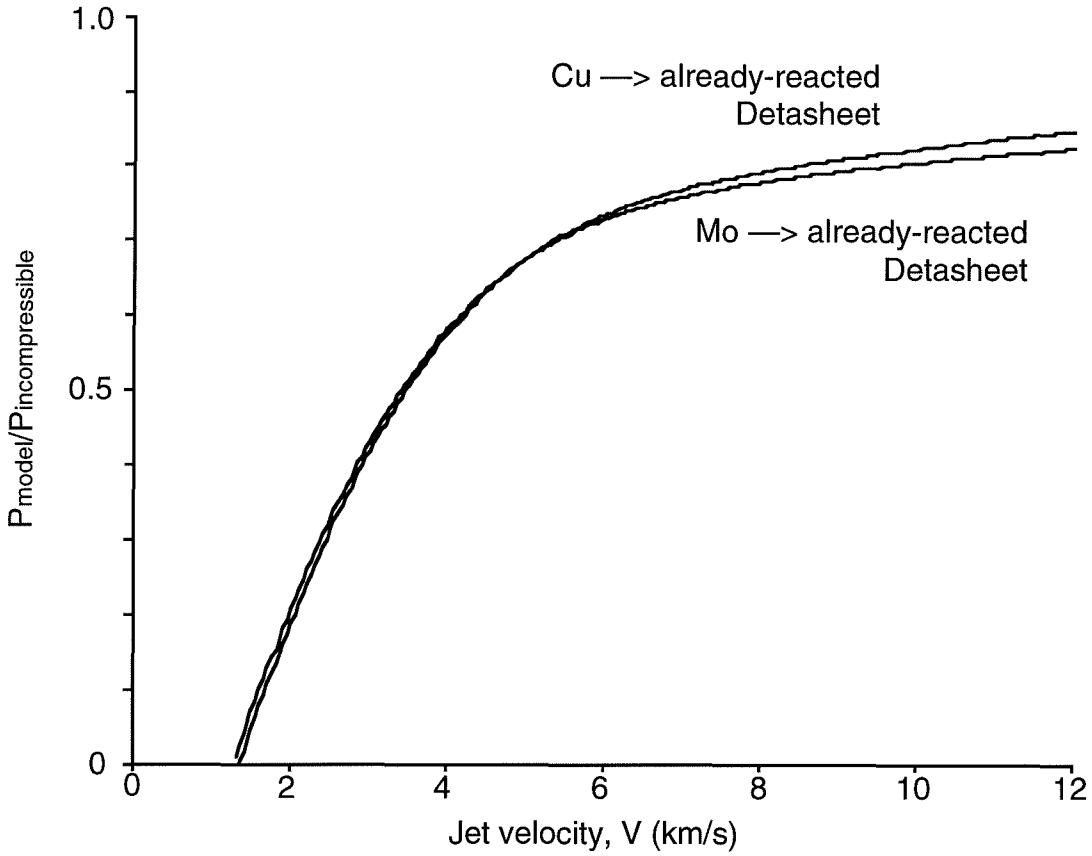

Figure 3. Model predictions of penetration per unit length of jet into already-reacted explosive (Case II), relative to the prediction of the incompressible density law.

Table 1. Material Properties Used in Model Computations.

	copper	molybdenum	Plexiglas	Detasheet	Comp. C-4
ρ_0 (Mg/m^3)	8.93	10.2	1.186	1.480	1.601
c_0 or D (km/s)	3.92	5.163	2.745	7.000	8.193
b	1.488	1.236	1.451	- -	- -
Γ_0 or γ	1.96	1.41	0.80	2.719	2.838

For Case I, we computed penetrations by high-velocity copper (Cu) and molybdenum (Mo) jets into Detasheet (EL-506C) explosive. In Fig. 2, these are compared with penetration by Cu jets into Plexiglas (PMMA), an inert compressible plastic with a low density like that of Detasheet. The explosive-target curves begin at jet velocities of about 10 km/s; for slower jets, the penetration velocity U would be less than the detonation velocity D and the Case I steady state would not be achieved.

In this figure, we observe, first, that the reduction in penetration in Detasheet relative to the density law is about 12% to 15%, which is about the same reduction attributed to compressibility alone in Plexiglas at these velocities. Second, the curves for Cu and Mo jets are not very different; this is because both metals are negligibly compressible compared with the explosive. Another difference is that Mo, which is denser than Cu,

has a greater penetration velocity U, so that it can keep up with the detonation wave and achieve a steady state at lower jet velocities; thus, its curve starts at a lower V.

For Case II of an already-reacted explosive target, Fig. 3 shows that penetration is most degraded relative to the density law at low velocities, where the gas's high initial pressure resists the jet's stagnation pressure; indeed, at the lowest velocities, the jet is unable to penetrate at all. At high velocities, this curve does not approach unity because of compressibility, but comes near the corresponding Case-I curve of Fig. 2. Thus, it seems that at high velocities, it matters little whether the explosive is reacting or has already reacted; that is, the compressibility of the product gases seems to account here for most of the deviation from the density law.

EXPERIMENTS

Experiments of shaped-charge jet penetration of explosives have been performed, as shown in Fig. 4. In each test, a precision 66-mm-diameter 42° conical copper-lined charge (V_{tip} = 9.14 km/s) was fired into a cylinder of Comp. C-4 explosive at a standoff of 198 mm. Six experiments were performed, listed in Table 2. Flash radiography recorded images of each jet during and after penetration. Analysis of the radiographs determined the tip velocity of the eroded jet after penetration. In one test (#4), we deliberately misaligned the shotline (penetration path) with the axis of the target charge; in two other tests (#2 and 3), we were able to observe a small, unintentional misalignment, which we believe did not significantly affect the results. In the last two tests, the target charge was confined by inserting it snugly into a hole in a 25.4-mm-thick aluminum plate and covering it top and bottom with 6-mm-thick steel plates.

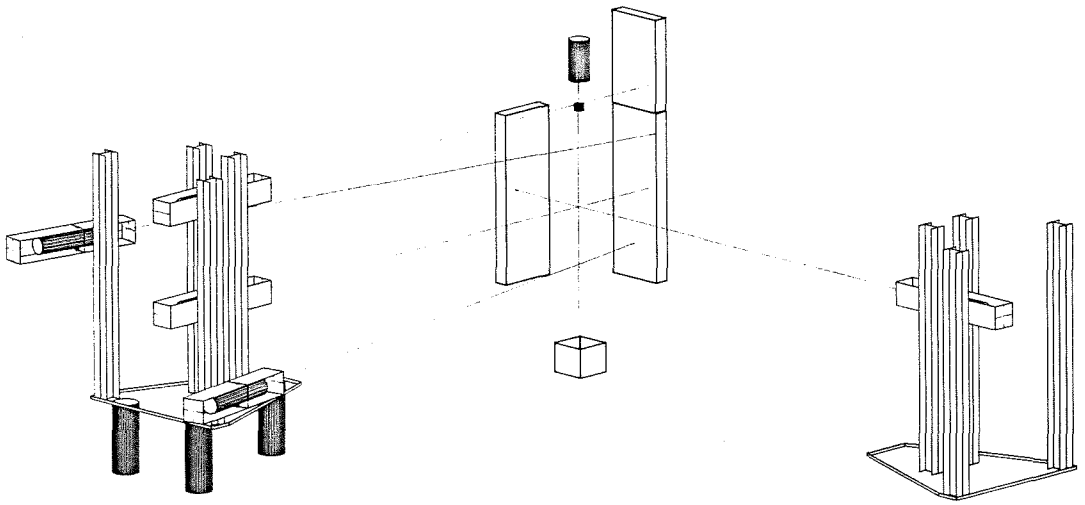

Figure 4. Setup of experiments of shaped-charge jet penetration of explosives.

In radiographs of the actual penetration process, it appears that eroded jet material is projected by the high-pressure explosive products back into the jet, disturbing it. We have also observed this in hydrocode computations of such penetrations, an example of which is shown in Fig. 5.

The behind-target radiographs showed that the explosive affected the jet in three regimes, as shown in Fig. 6: 1) the front part of the jet was eroded, that is, completely removed (this is addressed by our model); 2) the next portion of jet was greatly disrupted, with highly fragmented particles dispersed some distance off the shotline; and

Table 2. Experiments of shaped-charge jet penetration of explosive.

Test no.	*Explosive size length × diameter*	*Explosive confinement*	*Shotline offset*	*Residual jet velocities (km/s)* V_1	V_2	V_3
1	25.4 × 38.1 mm	none	0?	8.76	7.89	7.39
2	50.8 × 38.1 mm	none	2.7 mm	8.15	7.40	7.30
3	25.4 × 76.2 mm	none	3.2 mm	8.78	- -	7.42
4	25.4 × 38.1 mm	none	16.3 mm	- -	8.77	8.06
5	25.4 × 38.1 mm	heavy	0?	8.26	- -	6.40
6	25.4 × 38.1 mm	heavy	0?	7.86	- -	6.01

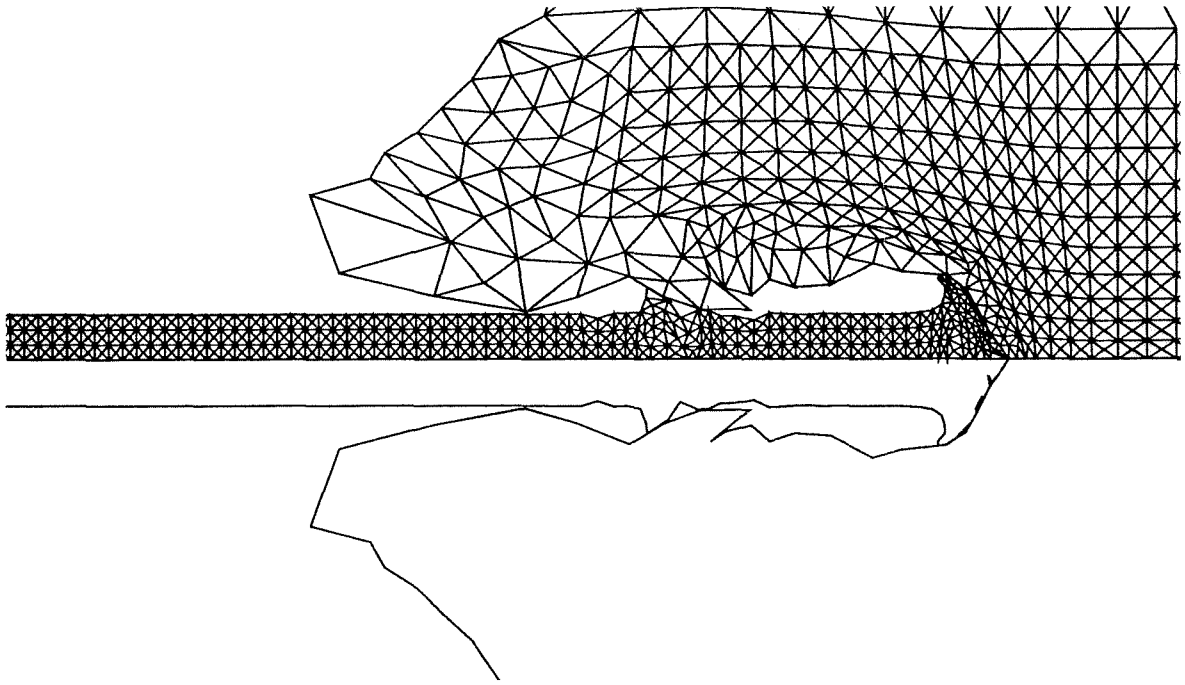

Figure 5. Hydrocode computation of penetration by a copper jet at 9 km/s into a target of C-4 explosive. Notice the disturbance of the jet along its sides.

3) a third part was sometimes deflected but still had the appearance of a jet and was only mildly broken. The rest of the jet was not noticeably affected. These effects are similar to phenomena observed by Brown and Finch[3] in confined sheet explosive. The approximate velocity points that divide the jet into these regimes are listed in Table 2.

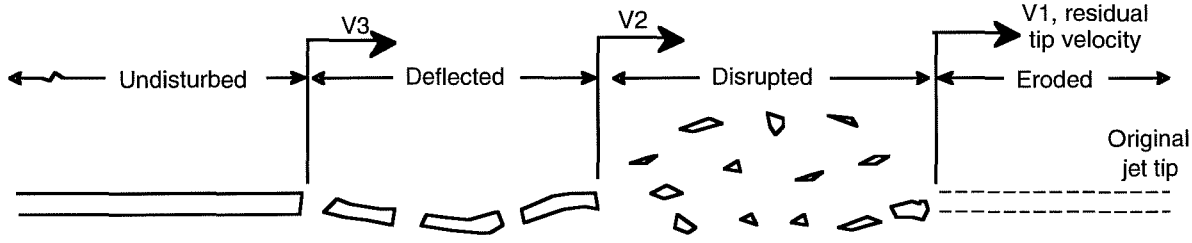

Figure 6. Regimes of jet disturbance by explosive penetration.

[3] J. Brown and D. Finch, "The Shaped Charge Jet Attack of Confined and Unconfined Sheet Explosive at Normal Incidence," *Proc. 11th Inter. Symp. Ballistics*, Brussels, 9-11 May 1989.

The model is compared with the results of Tests #1 and #2 in Fig. 7, which is a plot of residual jet tip velocity vs. thickness of explosive target. The Case II model was applied incrementally and integrated numerically over the jet to determine how much was eroded. The test data are the velocities of the fastest particles (usually disrupted or displaced) found in the post-target radiographs, as illustrated in Fig. 6. Agreement is excellent, provided that foreshortening of the jet is also taken into account. Our rule is that a length of jet equal to four times the jet diameter is lost due to foreshortening.

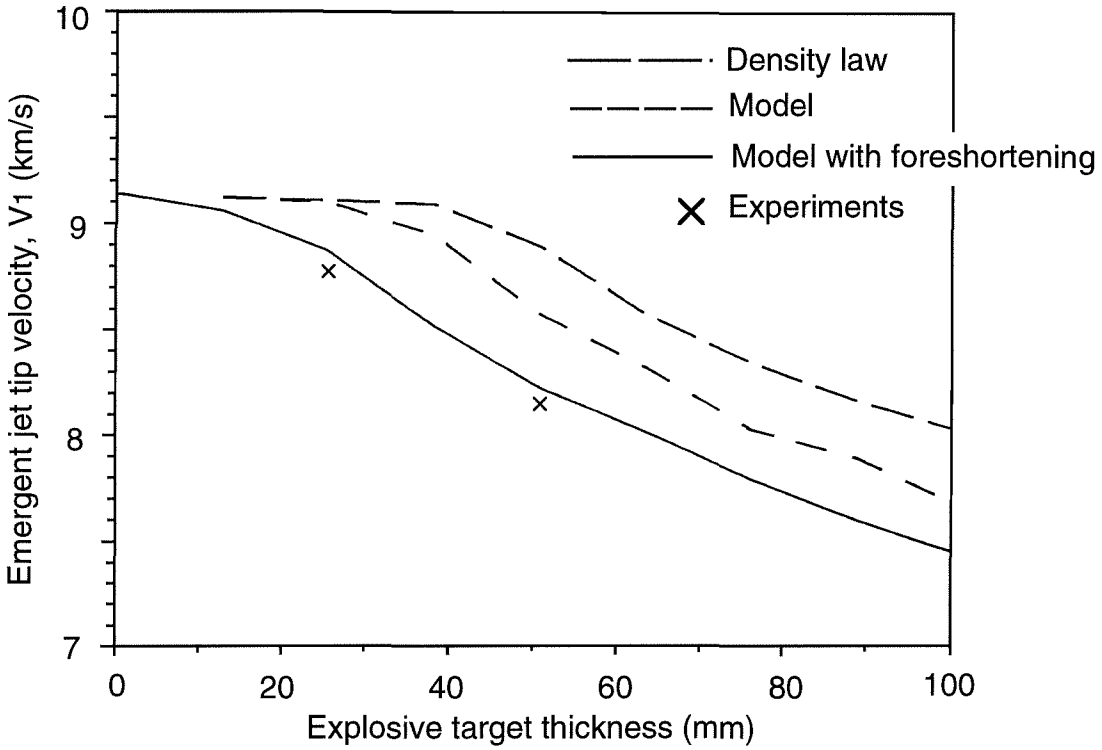

Figure 7. Comparison of Case II model with experimental results.

CONCLUSIONS

The 1-D steady-state approach of Haugstad and Dullum for compressible penetration by shaped-charge jets has been applied to explosive targets described by a γ-law equation of state. Separate models have been developed for high- and low-velocity jets.

Computed results show that for high-velocity jets, the predicted penetration is about 15% less than that predicted by the incompressible density law; this difference is similar to that attributed to compressibility in compressible inert targets, such as plastics and liquids. For low-velocity jets penetrating confined, already-reacted explosives (product gases), the high initial pressure of the explosive greatly resists penetration. Comparisons of this model with the results of some experiments show good agreement provided that foreshortening is also taken into account.

Experimental post-target radiographs showed three effects of explosive penetration on successive parts of the jet: erosion; disruption into a highly fragmented, dispersed state; and deflection off the shotline.